Journal of
Materials Chemistry B

Materials for biology and medicine

Accepted Manuscript

This article can be cited before page numbers have been issued, to do this please use: C. J. R. Wells, M. M. Rizk, J. R. Manning, D. Winning, C. Brambila, D. F. Brougham, F. Carniato, M. Botta, J. Wilton-Ely and G. Davies, *J. Mater. Chem. B*, 2026, DOI: 10.1039/D6TB01037G.

ROYAL SOCIETY OF CHEMISTRY

rsc.li/materials-b

View Article Online
DOI: 10.1039/D6TB01037G

ARTICLE

Exploring the influence of internal surface modification of paramagnetic mesoporous silica nanoparticles on MRI relaxation dynamics

Received 00th January 20xx,
Accepted 00th January 20xx

DOI: 10.1039/x0xx00000x

Connor J. R. Wells,[1,2] Marwa M. I. Rizk,[1,3] Joseph R.H. Manning,[1] Danielle Winning,[4] Carlos Brambila,[5] Dermot F. Brougham,[4] Fabio Carniato,[6] Mauro Botta,[6] James D. E. T. Wilton-Ely,[2] and Gemma-Louise Davies[1,7*]

Paramagnetic mesoporous silica nanoparticles (MSNs) containing immobilised Gd^{3+}-macrocycles are widely investigated as platforms for enhancing magnetic resonance imaging (MRI) contrast, yet the influence of the local chemical surface environment on relaxation dynamics remains underexplored. In this work, we systematically examine how internal surface functionalisation modulates the relaxometric behaviour of Gd^{3+}-chelate modified MSNs. Monodisperse MSNs were prepared with constant Gd^{3+} loading and varying either proximal thiol or phenyl groups. Thiol-functionalised particles exhibited a clear enhancement in relaxivity with high thiol grafting densities. Fast field-cycling NMR fitting parameters indicated that thiols progressively restrict local rotational dynamics, likely due to changes in local viscosity inside pores coupled with changes in the hydration layer structure around the Gd^{3+}-chelate, reaching a plateau once the grafting density exceeds the density of Gd^{3+}-chelates. In contrast, phenyl groups produce relaxivity enhancement through steric restrictions and hydrophobic crowding that limit chelate motion. Variable-temperature studies confirm that relaxation is dominated by local rotational dynamics rather than water exchange in both cases. These findings demonstrate that different surface modifiers enhance MRI performance *via* distinct mechanisms, highlighting internal surface chemistry as a key consideration in the design of nanoparticulate contrast agents.

Introduction

Contrast agents based on paramagnetic (usually Gd^{3+}-chelate) moieties are routinely used to enhance image clarity in magnetic resonance imaging (MRI). The structure-property relationship of contrast agents plays a crucial role in determining their MRI enhancement capabilities. For molecular contrast agents, this interplay of properties is well understood, with significant efforts over several decades contributing to a well-defined and experimentally-verified model of water dynamics with Gd^{3+}-chelate species.[1, 2]

Amongst numerous mechanistic strategies to enhance MRI contrast, including increasing hydration number (q) and modulating the water exchange lifetime (τ_M), increasing the rotational correlation time (τ_R) through increased mass or bulk has been consistently reported. A variety of approaches have been investigated to achieve this, with macromolecular and nanostructured species becoming popular bulky platforms for Gd^{3+}-chelates.[3-5] Mesoporous silica nanoparticles (MSNs), in particular, have been explored for a number of years as hosts for Gd^{3+}-chelates, with different approaches producing significant improvement in MRI contrast enhancement, as well as an understanding of design principles.[6-12] For example, the use of different chain linker lengths influences local rotational correlation time (τ_{RL}); long, flexible linkers allow greater local motion of the Gd^{3+}-chelates, reducing τ_{RL} and lowering per-Gd^{3+} relaxivity (r_1, relaxation rate enhancement per mM concentration of the agent), whereas shorter and more rigid linkers restrict local molecular motion, increasing τ_{RL} and boosting relaxivity.[7] The positioning of Gd^{3+}-chelates within the MSN structure influences water accessibility and relaxation efficiency. There have been conflicting reports for different mesopore structures and approaches, with some describing external surface anchored Gd^{3+}-chelates allowing better contact with bulk water and higher relaxivity, whereas location inside pores limits water exchange due to steric confinement, reducing relaxitivity;[9, 13] others, however, have reported better relaxometric properties when complexes were internally localised compared to external surface location, citing the influence of varying water dynamics.[11, 14, 15] The pore size and connectivity of the silica matrix also influence how easily water molecules can diffuse to and from the chelate sites: larger open

[1]*Department of Chemistry, University College London, 20 Gordon Street, London, WC1H 0AJ, UK*
[2]*Department of Chemistry, Molecular Sciences Research Hub, Imperial College London, 82 Wood Lane, London, W12 0BZ, UK*
[3]*Department of Pharmaceutics, Faculty of Pharmacy, Alexandria University, Alexandria, Egypt*
[4]*School of Chemistry, University College Dublin, Belfield, Dublin 4, Ireland*
[5]*School of Chemical, Materials and Biological Engineering, University of Sheffield, Mappin Street, Sheffield S1 3JD UK*
[6]*Dipartimento di Scienze e Innovazione Tecnologica, Università del Piemonte Orientale 'A. Avogadro', Alessandria, Italy*
[7]*School of Chemistry, University of Birmingham, Edgbaston, Birmingham, B15 2TT, UK*
Supplementary Information available: FTIR spectra, Ellman's assay calibration and data, gas sorption porosimetry. See DOI: 10.1039/x0xx00000x

View Article Online
DOI: 10.1039/D6TB01377C

pores facilitate water access and exchange, boosting relaxivity, while small or disconnected pores hinder this process.[16] The density of anchoring sites affects both immobilisation and hydration; higher anchor densities have been shown to rigidify chelates, improving τ_{RL}.[13]

Beyond the structure of MSNs and Gd^{3+}-chelate immobilisation strategy, it is important to note that the innate MSN porosity results in a significant surface area that is in close proximity with the immobilised Gd^{3+}-chelate species, particularly within the mesoporous network. It has been established that molecular Gd^{3+}-DOTA (DOTA= 1,4,7,10-tetraazacyclododecane-1,4,7,10-tetraacetic acid) and other chelate species in solution can interact with salts in a coordinative manner.[15,16] Similarly, the chemical environment of neighbouring MSN surfaces may significantly influence water interactions with surface-bound Gd^{3+}-chelates and thus, relaxivity. This was shown by Carniato *et al.*, who noted that reactive surface groups on MSNs near Gd^{3+}-chelates led to reduced relaxivities.[7] When protonated amino groups were present on MSN surfaces, low relaxivities were attributed to restricted accessibility of water molecules to the metal centre due to strong electrostatic interactions between the negatively charged Gd^{3+}-chelate and the cationic amino groups; converting these to neutral amides removed this electrostatic interaction, leading to a substantial increase in relaxivity. This illustrates that precise chemical control over surface functionality and chelate location can dramatically enhance relaxation behaviour. Despite the potential to modulate r_1 through the local chemical environment, there have been no further illustrations in the literature of the impact of local surfaces on the relaxation enhancement of Gd^{3+}-chelates hosted in MSNs.

Herein, we investigate the influence of local surface functionalisation on the MRI relaxometric behaviour of Gd^{3+}-chelate-modified MSN suspensions. By introducing different functional groups within the porous silica framework near the immobilised Gd^{3+}-DO3A monoamide chelates (DO3A = 1,4,7,10-tetraazacyclododecane-1,4,7-triacetic acid), we aim to gain insight into how these chemical environments modulate relaxation properties.

Results and discussion

MSNs were synthesised and their internal surfaces covalently grafted with Gd^{3+}-DO3A monoamide (Gd^{3+}-DO3Ama) chelates alongside functional silanes (either thiol ((3-mercapto)trimethoxysilane) or trimethoxyphenylsilane, schematically shown in Figure 1a).

Maintaining the Gd^{3+}-DO3Ama concentration the same (0.15 mol% with respect to silica), three thiol loading levels (0.5, 1, and 2 mol%) were prepared.

Nanoparticle characterisation

Transmission electron microscopy (TEM) demonstrated the size, morphology and homogeneity of each Gd^{3+}-DO3Ama loaded sample (Figure 1). Particle sizes ranged 41 – 49 nm (Table 1) and are comparable to literature reports of similarly prepared nanomaterials.[17, 18] Notably, the sizes all lie within error of one another, which is essential for reliably comparing the relaxometric behaviour independent of global rotational differences. Addition of thiol groups did not significantly affect the morphology or porosity of the particles. Dynamic light scattering (DLS) confirmed colloidal stability; all samples, regardless of functionalisation, displayed hydrodynamic diameters ranging 199 – 254 nm. The low polydispersity indices (PDI - obtained from DLS) observed for all suspensions (< 0.17) highlight their excellent monodispersity in aqueous media (Table 1).

Table 1. Hydrodynamic diameters and polydispersities (as measured by DLS of 0.5 mg/mL suspensions in ultrapure water) and mean particle sizes (according to TEM).

Sample	Hydrodynamic diameter (nm)	Polydispersity index"	Mean particle size‡ (nm)
Gd^{3+}-DO3Ama-MSNs	254 ± 3	0.15 ± 0.01	41 ± 5
Thiol-MSNs-0.5 mol%	214 ± 4	0.17 ± 0.03	46 ± 7
Thiol-MSNs-1 mol%	202 ± 7	0.10 ± 0.04	49 ± 4
Thiol-MSNs-2 mol%	199 ± 2	0.07 ± 0.01	46 ± 5

"Polydispersities (PDI) measured by DLS; ‡Values calculated from TEM images, where a minimum of 100 particles were measured using ImageJ software.

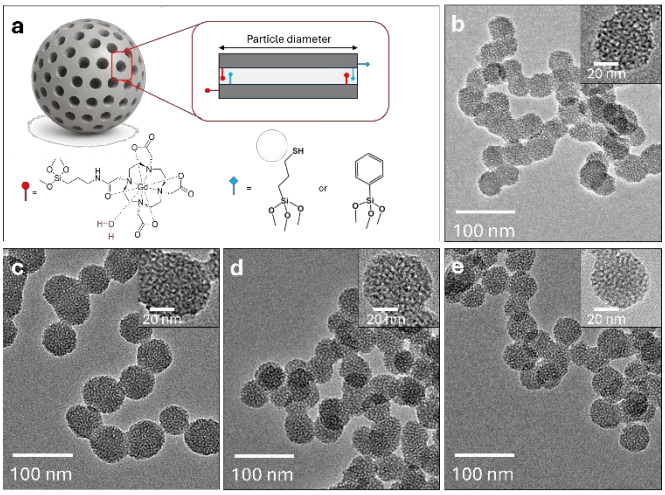

Figure 1. Schematic of grafted MSNs (a); transmission electron microscope images of unmodified Gd^{3+}-DO3Ama-MSNs (b), and thiol-modified Gd^{3+}-DO3Ama-MSNs at thiol loadings of 0.5, 1, and 2 mol% (c, d, e respectively).

Fourier-transform infrared (FTIR) spectroscopy (Fig. S1) showed characteristic Si-O-Si (1055 cm^{-1}, 795 cm^{-1}) and Si-OH (960 cm^{-1}) vibrations. Due to their low loading and subtle FTIR features, the grafted functional thiol groups and Gd^{3+}-DO3Ama could not be resolved. The presence of Gd^{3+} was confirmed using inductively coupled plasma-optical emission spectroscopy (ICP-OES), with Gd^{3+} levels all being within error (at 2.1-2.4 wt% with respect to SiO_2, Table S1). Thiol quantification was performed using Ellman's reagent (5,5'-dithio-bis-(2-nitrobenzoic acid), with thiol content calculated from the linear absorbance calibration curve (Figure S2). As shown in Figure S3, measured values closely matched theoretical loadings, corresponding to thiol

View Article Online DOI: 10.1039/D6TB01375C

contents of 0.46, 0.80, and 1.93 mol% (for 0.5, 1, and 2 mol% labelled samples, respectively).

Gas sorption porosimetry showed that all particles possess type IV N_2 adsorption-desorption isotherms (Figure S4) common for mesoporous materials, with hysteresis between 0.9 – 1 P/P_0. Surface areas determined using Brunauer-Emmet-Teller (BET) measurements (Table S2) were between 888 – 1080 m^2/g, typical of similar sized MSNs.[18] Pore diameters, as calculated by the Barret-Joyner-Halenda (BJH) method (Table S2), were ~3.1 nm for all nanoparticle types, as expected for this synthetic route.[11] Pore volumes were also calculated using the BJH method, with the range found between 0.72 – 0.81 cm^3/g. Importantly, the addition of extra surface (thiol) functionalities did not impact the measured porosity or pore size of the composites, with pores remaining intact and comparable surface areas.

MR Relaxation

Since ^1H relaxivity is strongly dependent on the observation frequency, measuring it across a broad range - typically from 0.01 to 120 MHz - provides a powerful approach to extract key structural and dynamic information regarding the metal centre of contrast agents.[19] These measurements are performed using specialised instrumentation, namely a fast field-cycling nuclear magnetic relaxometer (FFC-NMR). This technique enables the accurate, rapid, and sensitive acquisition of nuclear magnetic relaxation dispersion (NMRD) profiles.[20] For nanomaterials characterised by slow rotational dynamics, only the high field region (> ca. 5 MHz) can be accurately interpreted using Solomon-Bloembergen-Morgan (SBM) theory.[21] Relaxivity in the low frequency region of the NMRD profile is described by advanced models that incorporate both static and transient zero-field splitting (ZFS), which determine electron spin energy levels and the associated electron-nucleus transition probabilities.[22-24] When considering paramagnetic species attached to the surface of nanoparticles, as is the case here, both the global tumbling of the overall particle, and the local motion of the paramagnetic species itself must be considered. To reconcile these dynamics, the model-free Lipari-Szabo approach[25] can be used, which takes into account the local tumbling (τ_{RL}) of the Gd^{3+}-chelate anchored to MSNs and the global rotation (τ_{RG}) of the entire nanoparticle. The order parameter, S^2, represents the degree of spatial restriction or correlation between these two motions, ranging from zero (entirely independent motions) to one (fully correlated, rigid attachment). Several parameters were fixed to values established in previous studies - namely, the number of inner-sphere water molecules coordinated to the metal (q = 1) and the distance between Gd^{3+} and the bound water protons ($r_{Gd–H}$ = 3.0 Å) - and the NMRD profiles were subsequently fitted (Table 2).[2, 7, 10, 13, 26] Furthermore, the water diffusion coefficient at 310 K (^{310}D) and the distance of closest approach for outer-sphere water molecules ($a_{Gd–H}$) were kept constant throughout the analysis. It must be emphasized that the system is inherently complex, likely involving Gd^{3+}-chelates in various chemical environments and locations within the MSNs, such as the external surface, the pore interiors, or the pore entrances. Consequently, the relaxation parameters derived from the NMRD analysis represent weighted averages of these different populations. Nevertheless, despite this inherent complexity, valuable insights can still be extracted from the data.

^1H NMRD profile shapes (Figure 2) are typical of slowly-tumbling Gd^{3+}-chelate-modified proteins and other nanoscale systems, including MSNs, where the complexes are usually attached to the particle surfaces.[6, 10, 26-29] Thiol-modified MSNs displayed higher relaxivities across all frequencies compared to the unmodified Gd^{3+}-DO3Ama-MSNs. In particular, at higher frequency (ca. 30–80 MHz), into the clinical range, relaxivity increased with thiol content, with Thiol-MSNs-2 mol% presenting the highest relaxivity maximum (r_1 = 35.9 $mM^{-1}s^{-1}$ at 52 MHz). Due to the small pore size of the MSNs (3.0 – 3.1 nm), there is a tightly bound hydration layer adjacent to silanol surfaces inside the pores. This layer has been shown in literature to produce slowed τ_R and τ_D (diffusional correlation time), increasing interactions with Gd^{3+}-chelates and boosting relaxivity.[30-32] In our system, analysis of the NMRD profiles reveals that τ_{RL} is enhanced in the thiol-functionalised systems. As shown in Table 2, values for the 0.5-2 mol% Thiol-MSNs are higher than those of the unmodified Gd^{3+}-DO3Ama-MSNs, suggesting greater local rigidity. During the fitting process, the parameter τ_{RG} was fixed at 10 μs to account for the slow tumbling of the particles, in agreement with previous analyses of paramagnetic MSNs. Notably, the fit results are insensitive to variations in this parameter across a wide range (approximately 100 ns to 1 ms). Additionally, while the water exchange lifetime (τ_M) cannot be determined with high accuracy, the NMRD profiles of the various samples cannot be satisfactorily simulated unless the residence time of the coordinated water falls within the range of ~ 100-300 ns (310 K). This is consistent across all thiol-modified MSNs and indicates a slightly faster water exchange than for typical Gd^{3+}-DO3A monoamide derivatives.[33] The presence of thiol groups alters this confined water microenvironment through altering the hydration structure nearby the Gd^{3+} centre. As thiol groups can participate in weak hydrogen-bonding interactions and alter local surface polarity, their presence is likely to modify the structure and dynamics of confined water within the pores. Such changes may alter the local viscosity and hydration environment around the chelate, altering its local rotational dynamics and causing the boosts observed. Taking the error into consideration, τ_{RL} reaches a plateau above 0.5 mol%, which may reflect a saturation effect relative to the fixed Gd^{3+} loading (0.15 mol%). The S^2 order parameter shows a steady increase from the unmodified sample (0.12 ± 0.01), again plateauing to S^2 values within error for Thiol-MSNs-0.5 mol% – Thiol-MSNs-2 mol% (0.20 ± 0.01 – 0.25 ± 0.01). This indicates increased coupling between global and local rotation, corroborating that increasing thiol density alters the local dynamic environment around the immobilised chelates, with the effect limited by the relative ratio of Gd^{3+}:thiol groups. A slightly higher low frequency relaxivity is observed for the Thiol-1mol% sample, however this feature is not reflected in the fitted dynamic parameters and does not affect the overall trend observed across the series.

View Article Online
DOI: 10.1039/D5TB01577G

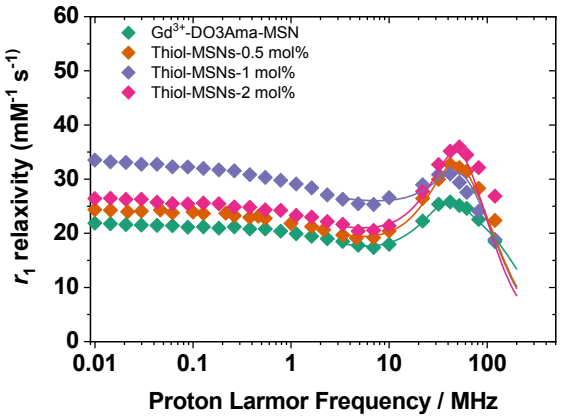

Figure 2. ^{1}H NMRD profiles (at 310 K) of Gd^{3+}-DO3Ama-MSNs and Thiol-MSNs. Fittings of the curves (solid lines) are calculated with the parameters in Table 2.

Table 2. Parameters obtained from the fits of ^{1}H NMRD data.

Sample/Parameter	τ_{RL} (ns)	S^2	τ_M (ns)
Gd^{3+}-DO3Ama-MSNs	0.9 ± 0.1	0.12 ± 0.01	160*
Thiol-MSNs-0.5 mol%	1.8 ± 0.2	0.20 ± 0.01	160*
Thiol-MSNs-1 mol%	1.9 ± 0.1	0.23 ± 0.01	160*
Thiol-MSNs-2 mol%	2.3 ± 0.5	0.25 ± 0.01	160*
Phenyl-MSNs-0.15 mol%	2.9 ± 0.8	0.30 ± 0.01	120*
Phenyl-MSNs-1mol%	2.2 ± 0.5	0.23 ± 0.01	160*

*Parameter fixed during fitting; other fixed parameters: τ_{RG} = 10 µs; q = 1; r_{GdH} = 3.0 Å; a_{GdH} = 4.0 Å; ^{310}D = 3.1 x 10^{-10} m^2s^{-1}.

As the hydrophilic thiol modifier appeared to reach a clear plateau in behaviour linked to the amount of Gd^{3+}-DO3Ama on the particles, MSNs modified with the more hydrophobic trimethoxyphenylsilane, which does not form hydrogen bonds with water, were prepared at 0.15 mol% and 1 mol% grafting levels to evaluate its local effect. The phenyl-modified MSNs showed similar physical characteristics to the thiol-modified particles, with similar sizes according to TEM (40 ± 5 nm for Phenyl-MSNs-0.15 mol% and 43 ± 4 nm for Phenyl-MSNs-1 mol%, Figure S5a and S5b) and DLS (210 ± 1 nm, with PDI 0.12 ± 0.03 for Phenyl-MSNs-0.15 mol%, and 184 ± 4 nm, with PDI = 0.10 ± 0.03 for Phenyl-MSNs-1 mol%), and Gd^{3+} loading levels (0.24 ± 0.09 mM, 2.7 wt% with respect to SiO_2 for Phenyl-MSNs-0.15 mol% and 0.24 ± 0.06 mM, 2.7 wt % for Phenyl-MSNs-1 mol%, Figure S1, SI). Gas sorption porosimetry also showed a BET surface area of 941 ± 11 m^2/g for Phenyl-MSNs-0.15 mol% and 1018 ± 12 m^2/g for Phenyl-MSNs-1 mol% (Figure S5c, Table S2), pore volume of 0.79 cm^3/g and pore diameter of 3.2 nm for Phenyl-MSNs-0.15 mol%, and pore volume of 0.78 cm^3/g and pore diameter of 3.0 nm for Phenyl-MSNs-1 mol%, in line with the thiol-modified MSNs.

The trend observed in the ^{1}H NMRD profiles (Figure 3) is slightly different to that observed with thiol modifiers. Increased r_1 values were observed for both phenyl-modified samples across all frequencies compared to the unmodified particles, and profile shapes are again similar to Gd^{3+}-DO3Ama-MSNs, with prominent maxima in the 30-120 MHz range. The fitting parameters calculated for phenyl-modified MSNs (Table 2) show significantly increased τ_{RL} compared to unmodified Gd^{3+}-DO3Ama-MSNs (2.9 ± 0.8 and 2.2 ± 0.5 for Phenyl-MSNs-0.15 mol% and Phenyl-MSNs-1 mol%, respectively, compared to 0.9 ± 0.1). In this case, the presence of the phenyl groups likely leads to steric and hydrophobic crowding, and regions of hydrophobic 'patches' that affect pore wetting local to the paramagnetic centres, essentially causing reorganisation of water near the chelate. Increased S^2 values were again observed (0.12 ± 0.01 for unmodified, 0.30 ± 0.01 for Phenyl-MSNs-0.15 mol%, and 0.23 ± 0.01 for Phenyl-MSNs-1 mol%), further reflecting this surface grafting behaviour, suggesting the influence of the hydrophobic groups and their engagement with nearby water around the Gd^{3+}-chelates.

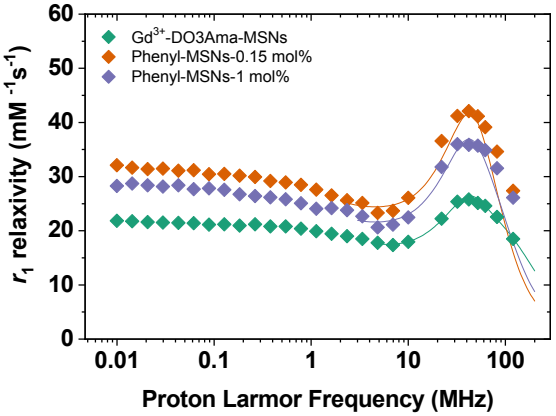

Figure 3. ^{1}H NMRD profiles (at 310 K) of Gd^{3+}-DO3Ama-MSNs and Phenyl-MSNs. Fittings of the curves (solid lines) are calculated with the parameters in Table 2.

Since the hydrophilic and hydrophobic pore environments may also influence water exchange behaviour, a temperature-dependence relaxometric study was performed on the thiol- and phenyl-modified MSNs prepared with the highest grafting levels, in order to ascertain which factors limit relaxivity in these systems.[7, 34] Small increases in r_1 with decreasing temperature were observed for both samples (Figure S6), indicating that these nanosystems operate within an efficient water exchange regime (intermediate to fast-exchange).[35] This suggests that relaxivity is primarily limited by local rotational motion rather than water exchange kinetics, directly corroborating the best-fit parameters presented in Table 2.

Conclusions

MSNs are widely investigated hosts for Gd^{3+}-chelate species due to their high surface areas and capacity for functionalisation, producing MRI contrast agents with enhanced relaxometric properties.[9, 11, 13-15] Their high surface areas are often employed to graft additional functionalities, with a view to multi-functionality and inclusion of targeting species. However, their internal pore surfaces also provide a chemically tuneable environment in close proximity to immobilised paramagnetic centres, offering opportunities to modulate water dynamics and relaxivity beyond that accessible through the properties of

the chelate itself. In this study, we demonstrate that the local chemical environment within the mesopores plays an important role in governing the relaxometric behaviour of immobilised Gd^{3+}-chelates. By varying proximal functional groups through the addition of low amounts of thiol and phenyl moieties, whilst maintaining constant Gd^{3+} loading and pore architecture, we highlight the influence of local surface functionality on MRI relaxivity.

Relaxometric analyses reveal that surface functionalisation primarily influences the local rotational dynamics of the immobilised chelates, regardless of the functional group. For thiol-modified MSNs, the fitted parameters indicate progressive increases in τ_{RL} and S^2 relative to the unmodified system, reflecting greater restriction of local chelate motion and stronger coupling between local and global rotational dynamics. These changes are consistent with modification of the interfacial environment within the confined mesopores, where polar surface functionalities influence dynamics of water adjacent to the silica surface and consequently alter the effective mobility of the surface-bound complexes. The trend approaches a plateau above 0.5 mol%, suggesting saturation relative to the fixed Gd^{3+} loading.

Phenyl functionalisation leads to similarly elevated τ_{RL} and S^2 values, however, this arises from a different local environment within the pores. The introduction of hydrophobic phenyl groups creates regions of increased steric crowding and hydrophobic character within the pore space. This environment is likely to influence pore wetting, leading to local reorganisation of water which restricts the local tumbling of the chelates and enhances r_1 at all grafting densities.

Overall, these results highlight that relaxivity enhancement in Gd^{3+}-chelate modified MSNs is not solely dictated by the chelate itself, but is strongly influenced by the surrounding surface chemistry adjacent to the Gd^{3+}-species within nanoscale pores. Precise control over local functional groups therefore represents a powerful and underexplored strategy for optimising MRI contrast agents and tailoring their dynamic behaviour.

Experimental

Materials

Cetyl trimethylammonium bromide (CTAB), tetraethyl orthosilicate (TEOS), triethanolamine, (3-aminopropyl)triethoxysilane (APTES), triethylamine, gadolinium(III) chloride, (3-mercapto)trimethoxysilane, trimethoxyphenylsilane, 5,5'-dithio-bis-(2-nitrobenzoic acid) (Ellman's reagent), L-cysteine hydrochloride, disodium phosphate, monosodium phosphate, ethylenediaminetetraacetic acid (EDTA), hydrochloric acid (HCl, 37%), and nitric acid (HNO3, 70%) were purchased from Sigma-Aldrich or Fisher Scientific. 2,2',2''-(10-(2-((2,5-dioxopyrrolidin-1-yl)oxy)-2-oxoethyl)-1,4,7,10-tetraazacyclododecane-1,4,7-triyl)triacetic acid (DO3A-NHS-ester) was purchased from CheMatech. A 10-element custom mix ICP standard was purchased from QMX Laboratories, containing Gd (100 mg/L) in 5% HNO_3 (100 mL). Dimethylformamide (DMF) and ethanol (EtOH) were used as received and sourced from Fisher Scientific or Sigma-Aldrich, UK. An Elga PureLab system operated at 16.0 MΩ or a Merck Milli-Q Direct water purification system operated at 18.2 MΩ provided the ultrapure water.

Instrumentation

Field-dependent relaxometry data were acquired on a 0.25 T SMARtracer relaxometer (Stelar) for magnetic fields between 0.01 – 10 MHz, and an HTS-110 3T Magnet System (Stelar) for magnetic fields from 10 MHz to 130 MHz, operated at 310 K. T_1 (using the inversion-recovery method) values were converted to r_1 relaxivities using equation 1, where [Gd^{3+}] in mM was acquired from inductively coupled plasma optical emission spectroscopy (ICP-OES).

$$r_1 = \frac{R_{1,obs} - R_{1,sol}}{[CA]} \quad (1)$$

Where r_1 is relaxivity, $R_{1,obs}$ is the observed longitudinal relaxation rate of the agent in aqueous suspension ($R_1 = 1/T_1$), $R_{1,sol}$ is the relaxation rate of the blank solvent system in the absence of contrast agent, and [CA] is the mM concentration of the contrast agent in aqueous suspension, as measured by ICP-OES. Samples were prepared for ICP-OES by digesting with hot nitric acid (70%), and diluting to 25 mL. ICP-OES was performed on an Agilent Varian 720-ES ICP-OES, running at 1 kW power with a 40 MHz radiofrequency argon plasma. The plasma gas flow was 15 L min^{-1}, and the nebuliser flow rate was 0.75 L min^{-1}. A calibration of 2 – 8 ppm was generated using a standard solution (QMX Laboratories). Gas sorption porosimetry was carried out on a Micromeritics TriStar at 77 K. BET surface areas and BJH pore sizes and volumes were obtained from Micromeritics software (model MicroActive 4.06).

An Agilent Cary 4000 UV-Vis spectrometer was used to record UV-vis spectra. DLS data, including hydrodynamic diameters and polydispersity indices were obtained from a Malvern Zetasizer Nano ZS at 25 °C. A 4 mW He-Ne laser at 633 nm was used, and scattered light was collected at 173°. Samples were dispersed in ultrapure water (0.5 mg/mL). Measurements were repeated three times. Transmission electron microscopy (TEM) images were acquired using a Jeol 2100Plus microscope, with 0.14 nm resolution, operated at 200 kV. Samples dispersed in ethanol were deposited onto a formvar-coated 300 mesh copper TEM grid and allowed to air dry. ImageJ software (version 1.52a) was used to measure particle size and averages were obtained from analysis of at least 100 particles. IR spectra of powdered solids were acquired on a Shimadzu IRTracer-100 FTIR spectrometer operated in ATR mode.

Synthesis of aminated and functionalised mesoporous silica nanoparticles (MSNs)

MSNs were prepared using a modified literature procedure:[11] CTAB (0.64 g, 1.75 mmol) was dissolved in a mixture of ultrapure water (16.02 mL, 0.89 mmol) and EtOH (1.84 mL, 0.03 mol), which was heated to 80 °C. Triethanolamine (1.03 g, 6.90 mmol) was added during stirring. TEOS (1.45 mL, 6.49 mmol) was added drop-wise, and the solution was allowed to stir for 1 h.

After this time, a mixture of TEOS (2.2 µL), APTES (2.3 µL) and either (3-mercapto)trimethoxysilane or trimethoxyphenylsilane (1.8, 6.0, 12.0, or 24.0 µL for samples 0.15 mol%, 0.5 mol%, 1 mol% and 2 mol%, respectively) was added. The solution was stirred for 1 h. The resulting suspension was centrifuged (15,000 rpm for 20 mins) and washed with acidic ethanol (20 mL EtOH: 3 mL HCl, 13.1 M). The MSNs were finally washed in EtOH until neutral pH was obtained. MSNs were stored in EtOH at room temperature. Samples without a functional group were prepared by omitting (3-mercapto)trimethoxysilane or trimethoxyphenylsilane from the procedure.

To load with Gd^{3+}, MSNs were dispersed in anhydrous DMF (12 mL). DO3A-NHS-ester (4 mg, 5 µmol) and triethylamine (200 µL) were added, and the reaction was stirred overnight (~16 h) at room temperature. The DO3Ama-loaded MSNs were washed twice with EtOH *via* centrifugation and sonication and re-dispersed in EtOH (10 mL). $GdCl_3$ (2.6 mg, 1 x 10^{-5} mol) was added and the solution stirred for 24 h at room temperature. Dialysis (3.5 KDa MWCO, 35 mm), followed by centrifugation washing was then carried out before storage in fresh EtOH for storage.

Thiol assays

A reaction buffer (RB) of phosphate buffer solution at 0.1 M, pH 8.0 (1 M Na_2HPO_4 and 1 M NaH_2PO_4 solutions, diluted to 1 L), containing 1 mM EDTA, was prepared. A calibration curve was obtained by preparing standards ranging from 0.1 mM to 1.6 mM of L-cysteine hydrochloride in RB, and absorbances were recorded at 412 nm (Figure S2). Ellman's reagent (4 mg) was dissolved in 1 mL RB, then 50 µL of this solution was mixed with 2.5 mL of RB. 250 µL of standard and/or sample (2 mg/mL of MSNs) was added to the diluted Ellman's reagent. The solutions were then mixed and incubated for 15 min at room temperature before UV-vis measurement.

Author contributions

Connor J. R. Wells: Data curation, Formal analysis, Investigation, Methodology, Writing – Original draft. **Marwa M. I. Rizk:** Investigation, Methodology. **Joseph R. H. Manning:** Supervision. **Danielle Winning:** Data curation. **Carlos Brambila:** Data curation. **Dermot F. Brougham:** Formal analysis, Writing – review & editing. **Fabio Carniato:** Data curation, Formal analysis, Writing – review & editing. **Mauro Botta:** Formal analysis, Writing – review & editing. **James D. E. T. Wilton-Ely:** Funding acquisition, Project administration, Supervision, Writing – review & editing. **Gemma-Louise Davies:** Conceptualisation, Funding acquisition, Project administration, Supervision, Writing – review & editing.

Conflicts of interest

There are no conflicts to declare.

Data availability

Raw datasets are available open access at https://doi.org/10.25500/edata.bham.00001671.

View Article Online DOI: 10.1039/D6TB01037G

Acknowledgements

CJRW thanks the EPSRC Centre for Doctoral Training in the Advanced Characterisation of Materials (EP/L015277/1) for funding. MMIR thanks the Missions sector in the Egyptian Ministry of Higher Education and the British Council Egypt for funding as a part of the Newton-Mosharafa scheme, as well as the Department of Chemistry at UCL for financial support. We are grateful to the EPSRC Centre for Doctoral Training in the Smart Medical Imaging (EP/L015226/1) for provision of a benchtop 0.25 T SMARtracer relaxometer.

References

1. G.-L. Davies, I. Kramberger and J. J. Davis, *Chemical Communications*, 2013, **49**, 9704-9721.
2. P. Caravan, *Chemical Society Reviews*, 2006, **35**, 512-523.
3. E. Gianolio, G. B. Giovenzana, D. Longo, I. Longo, I. Menegotto and S. Aime, *Chemistry – A European Journal*, 2007, **13**, 5785-5797.
4. J. Rudovský, P. Hermann, M. Botta, S. Aime and I. Lukeš, *Chemical Communications*, 2005, DOI: 10.1039/B418712A, 2390-2392.
5. E. Boros and P. Caravan, *Journal of Medicinal Chemistry*, 2013, **56**, 1782-1786.
6. F. Carniato, L. Tei and M. Botta, *European Journal of Inorganic Chemistry*, 2018, **2018**, 4936-4954.
7. F. Carniato, L. Tei, M. Cossi, L. Marchese and M. Botta, *Chemistry – A European Journal*, 2010, **16**, 10727-10734.
8. K. M. L. Taylor, J. S. Kim, W. J. Rieter, H. An, W. Lin and W. Lin, *Journal of the American Chemical Society*, 2008, **130**, 2154-2155.
9. K. M. L. Taylor-Pashow, J. D. Rocca and W. Lin, *Nanomaterials*, 2012, **2**, 1-14.
10. F. Carniato, M. Muñoz-Úbeda, L. Tei and M. Botta, *Dalton Transactions*, 2015, **44**, 17927-17931.
11. J. J. Davis, W.-Y. Huang and G.-L. Davies, *Journal of Materials Chemistry*, 2012, **22**, 22848-22850.
12. W.-Y. Huang, G.-L. Davies and J. J. Davis, *Chemical Communications*, 2013, **49**, 60-62.
13. F. Carniato, L. Tei, A. Arrais, L. Marchese and M. Botta, *Chemistry – A European Journal*, 2013, **19**, 1421-1428.
14. D. Şen Karaman, D. Desai, J. Zhang, S. Tadayon, G. Unal, J. Teuho, J. Sarfraz, J.-H. Smått, H. Gu, T. Näreoja and J. M. Rosenholm, *Journal of Materials Chemistry B*, 2016, **4**, 1720-1732.
15. J. S. Ananta, B. Godin, R. Sethi, L. Moriggi, X. Liu, R. E. Serda, R. Krishnamurthy, R. Muthupillai, R. D. Bolskar, L. Helm, M. Ferrari, L. J. Wilson and P. Decuzzi, *Nat Nanotechnol*, 2010, **5**, 815-821.
16. F. Carniato, L. Tei, W. Dastrù, L. Marchese and M. Botta, *Chemical Communications*, 2009, DOI: 10.1039/B820591D, 1246-1248.
17. J. Kobler, K. Möller and T. Bein, *ACS Nano*, 2008, **2**, 791-799.
18. K. Möller, J. Kobler and T. Bein, *Journal of Materials Chemistry*, 2007, **17**, 624-631.
19. S. Aime, M. Botta, D. Esteban-Gómez and C. Platas-Iglesias, *Molecular Physics*, 2019, **117**, 898-909.
20. S. H. Koenig and R. D. Brown, *Progress in Nuclear Magnetic Resonance Spectroscopy*, 1990, **22**, 487-567.

View Article Online
DOI: 10.1039/D6TB01037G

21. M. F. Ferreira, B. Mousavi, P. M. Ferreira, C. I. O. Martins, L. Helm, J. A. Martins and C. F. G. C. Geraldes, *Dalton Transactions*, 2012, **41**, 5472-5475.
22. I. Bertini, J. Kowalewski, C. Luchinat, T. Nilsson and G. Parigi, *The Journal of Chemical Physics*, 1999, **111**, 5795-5807.
23. J. Kowalewski, Kruk, D., Parigi, G. , *Adv. Inorg. Chem.*, 2005, **57**, 41-104.
24. I. Bertini, Galas, O., Luchinat, C., Parigi, G., *J. Magn. Reson., Ser. A*, 1995, **113**, 151-158.
25. G. Lipari and A. Szabo, *Journal of the American Chemical Society*, 1982, **104**, 4559-4570.
26. F. Carniato, D. Alberti, A. Lapadula, J. Martinelli, C. Isidoro, S. Geninatti Crich and L. Tei, *Journal of Materials Chemistry B*, 2019, **7**, 3143-3152.
27. G. Licciardi, D. Rizzo, M. Salobehaj, L. Massai, A. Geri, L. Messori, E. Ravera, M. Fragai and G. Parigi, *Bioconjugate Chemistry*, 2022, **33**, 2411-2419.
28. M. A. Kaster, M. D. Levasseur, T. G. W. Edwardson, M. A. Caldwell, D. Hofmann, G. Licciardi, G. Parigi, C. Luchinat, D. Hilvert and T. J. Meade, *ACS Applied Bio Materials*, 2023, **6**, 591-602.
29. L. Moriggi, C. Cannizzo, C. Prestinari, F. Berrière and L. Helm, *Inorganic Chemistry*, 2008, **47**, 8357-8366.
30. A. A. Milischuk and B. M. Ladanyi, *The Journal of Chemical Physics*, 2011, **135**.
31. S. Takahara, N. Sumiyama, S. Kittaka, T. Yamaguchi and M.-C. Bellissent-Funel, *The Journal of Physical Chemistry B*, 2005, **109**, 11231-11239.
32. I. Brovchenko, A. Geiger and A. Oleinikova, *The Journal of Chemical Physics*, 2004, **120**, 1958-1972.
33. B. N. Siriwardena-Mahanama and M. J. Allen, *Molecules*, 2013, **18**, 9352-9381.
34. H. Skår, J. G. Seland, Y. Liang, N. Å. Frøystein, K. W. Törnroos and R. Anwander, *European Journal of Inorganic Chemistry*, 2013, **2013**, 5969-5979.
35. M. Botta and L. Tei, *European Journal of Inorganic Chemistry*, 2012, **2012**, 1945-1960.

DOI: 10.1039/D6TB01037G

Exploring the influence of internal surface modification of paramagnetic mesoporous silica nanoparticles on MRI relaxation dynamics

Connor J. R. Wells[1,2], Marwa Rizk[1,3], Joseph R.H. Manning[1], Danielle Winning,[4] Carlos Brambila,[5] Dermot F. Brougham,[4] Fabio Carniato,[6] Mauro Botta,[6] James D. E. T. Wilton-Ely,[2] and Gemma-Louise Davies[1,7*]

[1] Department of Chemistry, University College London, 20 Gordon Street, London, WC1H 0AJ, UK

[2] Department of Chemistry, Molecular Sciences Research Hub, Imperial College London, 82 Wood Lane, London, W12 0BZ, UK

[3] Department of Pharmaceutics, Faculty of Pharmacy, Alexandria University, Alexandria, Egypt

[4] School of Chemistry, University College Dublin, Belfield, Dublin 4, Ireland

[5] School of Chemical, Materials and Biological Engineering, University of Sheffield, Mappin Street, Sheffield S1 3JD UK

[6] Dipartimento di Scienze e Innovazione Tecnologica, Università del Piemonte Orientale 'A. Avogadro', Alessandria, Italy 5301 2802 3701 6012

[7] School of Chemistry, University of Birmingham, Edgbaston, Birmingham, B15 2TT, UK

**Corresponding author's email: g.davies.7@bham.ac.uk*

Data availability statement

Raw datasets are available at https://doi.org/10.25500/edata.bham.00001671.